

VLC-Assisted Safety Message Dissemination in Roadside Infrastructure-Less IoV Systems: Modeling and Analysis

Yuncong Xie, *Student Member, IEEE*, Dongyang Xu, *Member, IEEE*, Tiantian Zhang, *Student Member, IEEE*, Keping Yu, *Member, IEEE*, Amir Hussain, *Senior Member, IEEE* and Mohsen Guizani, *Fellow, IEEE*

Abstract—Internet-of-vehicles (IoV) is an emerging paradigm with significant potential to improve traffic efficiency and driving safety. Here, we focus on the design of a novel visible light communication (VLC)-assisted scheme to enable driving safety-related IoV services that require ultra-reliable and low-latency communications (URLLC). Specifically, the vehicle-to-vehicle (V2V) communication mode is adopted to satisfy the ultra-low latency requirement of URLLC in roadside infrastructure-less IoV systems. In the outdoor V2V-VLC scenarios, the quality of the received optical signal is degraded by path loss, atmospheric turbulence and additive noise. In addition, the short-packet feature of URLLC introduces inevitable data decoding errors and imperfect channel state information (CSI). Against this background, we aim to investigate the reliability performance of URLLC in outdoor V2V-VLC systems, which is described by the average packet loss probability under given user-plane transmission latency. Firstly, we consider the ideal case of a perfect CSI at receiver, and derive an analytical expression of average packet loss probability. Further, a closed-form approximation is provided to simplify the numerical calculation. Next, we extend the theoretical analysis to a practical V2V-VLC system with imperfect CSI at the receiver. Through numerical results, we validate the accuracy of our designed theoretical framework and propose some preliminary ideas to enable driving safety-related IoV services in outdoor V2V-VLC systems.

Index Terms—IoV, URLLC, short-packet, visible light communication, vehicle-to-vehicle.

Copyright (c) 20xx IEEE. Personal use of this material is permitted. However, permission to use this material for any other purposes must be obtained from the IEEE by sending a request to pubs-permissions@ieee.org.

The work of Dongyang Xu was supported in part by the Open Research Fund of National Mobile Communications Research Laboratory, Southeast University (No. 2023D13), in part by the National Natural Science Foundation of China under the Grants No. 62001368, and also in part by the Key Research and Development Program of Shaanxi under Grant No. 2022GY-093. The work of Keping Yu was supported by JSPS KAKENHI Grant Number JP21K17736. (*Corresponding author: Dongyang Xu*)

Yuncong Xie and Tiantian Zhang are with School of Information and Communications Engineering, Xi'an Jiaotong University, Xi'an 710049, China (e-mails: qy1z29@stu.xjtu.edu.cn, tiantianzhang@stu.xjtu.edu.cn).

Dongyang Xu is with the School of Information and Communications Engineering, Xi'an Jiaotong University, Xi'an 710049, China, and also with National Mobile Communications Research Laboratory, Southeast University, Nanjing 211189, China (e-mail: xudongyang@xjtu.edu.cn).

Keping Yu is with the Graduate School of Science and Engineering, Hosei University, Tokyo 184-8584, Japan. (email: keping.yu@ieee.org).

Amir Hussain is with School of Computing, Edinburgh Napier University, Edinburgh, UK. (email: A.Hussain@napier.ac.uk).

Mohsen Guizani is with the Machine Learning Department, Mohamed Bin Zayed University of Artificial Intelligence (MBZUAI), UAE (email: mguizani@ieee.org).

Manuscript received XXX, XX, 2023; revised XXX, XX, 2023.

I. INTRODUCTION

In recent years, the road traffic injuries caused by the human operation errors have become one of the main components of accidental death around the world [1]. To overcome this global issue, the concept of Internet-of-vehicles (IoV) is proposed as a promising solution, which attempts to realize the cooperation, connectivity and automation of vehicle nodes [2], [3]. With the aid of IoV communications, the intelligent vehicles can deliver real-time information (e.g., road conditions, route suggestions and emergency alerts) with other vehicles and roadside units, and coordinate to improve the traffic efficiency and road safety. As one of the key technologies for the implementation of IoV, the vehicle-to-vehicle (V2V) communication is a compelling paradigm to enable the driving safety-related IoV applications (e.g., cooperative awareness and emergency warning) with the millisecond-level latency requirement and ultra-high reliability constraint of 99.999% and above. In fact, the aforementioned driving safety-related V2V scenarios can be classified into the category of ultra-reliable and low-latency communications (URLLC), which is envisioned as one of major paradigms for supporting numerous mission-critical Internet-of-Things (IoT) applications in the 5G wireless networks [4]–[6].

To guarantee the stringent latency and reliability constraints of URLLC in vehicular networks, there have been some related works [7]–[11] focused on this challenging issue and provided several constructive solutions. For instance, the authors in [7] analyzed the negative impact of fast-varying channel state due to the high mobility in vehicular networks, and then developed a twin-timescale radio resource allocation framework to reduce the frequency of instantaneous channel estimation, while minimizing the required transmission latency of all vehicular users. The authors in [8] focused on the research of high throughput-oriented transmission design for URLLC in a hybrid mmWave and sub-6GHz vehicular network, and proposed a directional vehicle algorithm for this circumstance. Moreover, the authors in [9] introduced a novel Markov chain model to characterize the end-to-end transmission behaviors of URLLC in vehicular networks, and the corresponding link adaptation protocol was developed to maximize the network throughput while ensuring the latency and reliability constraints. Also, the authors in [10] focused on the reliability analysis and learning-based resource allocation for URLLC in the V2V wireless network, where the tail distributions of real-time queue length were investigated to describe the overall reliability in this scenario. Meanwhile, the authors in [11] studied the issue of URLLC-aware computation

offloading in a space-assisted vehicular network, and designed an asynchronous deep reinforcement learning-based algorithm to maximize the average throughput of this system. Obviously, the aforementioned URLLC-oriented transmission strategies in the finite blocklength regime are based on the radio frequency (RF) technologies, which seem to be sufficient to ensure the requirement of driving safety-related V2V scenarios at the time being. However, with the growing market penetration of V2V solutions, the limited RF spectrum is unaffordable for URLLC in high-density road traffic scenarios.

As a powerful alternative to the existing RF-based solutions, the visible light communication (VLC) technology is regarded as a promising paradigm for enabling V2V applications in the future ITSs [12]–[14]. In typical V2V-VLC system, the vehicle uses its own light-emitting diode (LED)-based headlights and taillights as optical transmitters, and installs the photodetectors as receivers [15]. Specifically, the V2V-related information is delivered in the form of modulated optical data signal, which uses the visible light spectrum with wavelength of 380-780nm as the carrier. Compared to the RF-based solutions, the V2V-VLC paradigm has significant advantages such as large system bandwidth, anti-electromagnetic interference, high data rate and low infrastructure cost [16]. However, the aforementioned advantages of V2V-VLC scheme are highly dependent on the line-of-sight (LOS) propagation, which is not always available in the V2V system due to the mobility of vehicle nodes. Apart from this, the performance of V2V-VLC system is degraded by some negative impacts of the outdoor environment, such as atmospheric turbulence [17] and solar irradiance [18]. Hence, the URLLC-oriented transmission strategies for outdoor V2V-VLC system should be meticulously designed.

A. Literature Review

With the deployment of emerging vehicular communication, networking and sensing technologies, the issue of road safety in the IoV has received extensive attention from both academia and industry [19]. Against this background, the V2V communication provides some use cases with the potential to improve road safety and prevent traffic accidents, such as the exchange of basic safety messages (BSMs) and/or cooperative awareness messages (CAMs) [20]. The research scope of this manuscript is confined to the VLC-assisted safety message dissemination in the roadside infrastructure-less IoV system. Around this issue, there have been some representative works analyzed the system performance and presented constructive solutions. For example, the authors in [21] considered the V2V-VLC system with randomly distributed interferers, and analyzed the outage performance of this system via leveraging the tool of stochastic geometry. Also, the authors in [22] provided a comprehensive channel modeling and performance analysis for outdoor V2V-VLC systems with random lateral shift between the transmitter and receiver. Specifically, the outage probability and diversity-multiplexing tradeoff of outdoor V2V-VLC system was studied in [22], where the negative impacts due to path loss, shadowing and atmospheric turbulence were jointly considered. Moreover, the authors in [23] presented outdoor measurement results to reveal how the dynamic road traffic impacts the performance of

V2V-VLC systems, including the average bit error rate (BER) and average inter-vehicular distance. Considered the impact of vehicle headlight radiation pattern on the system performance, the authors in [24] established a statistical path loss model to characterize the large-scale fading of vehicular VLC channels with dynamic road traffic. The authors in [25] investigated the performance of V2V-VLC systems in the presence of sunlight noise, and the authors in [26] developed an extended-Kalman filter to mitigate the negative impact of sunlight noise. On the other hand, the multi-hop relaying technology is beneficial to improve the received signal-to-noise ratio (SNR) of modulated optical data signal, thanks to the cooperative diversity gain. In view of this, the authors in [27] and [28] respectively analyzed the BER and coverage range of multi-hop V2V-VLC systems under different weather conditions, and verified that the multi-hop relaying can provide a significant performance gain.

In typical URLLC-related scenarios, the data transmission is performed in the form of short packets to acquire an extremely low user-plane transmission latency (e.g., less than 1ms). From an information-theoretical perspective, the short-packet feature of URLLC will introduce an unavoidable decoding error under arbitrarily high SNR regime [29]. Apparently, the short-packet feature is not considered in the aforementioned literatures, and thus cannot be employed for the URLLC-oriented transmission design. Hence, the theoretical analysis for URLLC in the V2V-VLC system requires a novel methodology distinct from that utilized in [21]–[28]. Apart from the short-packet feature, the extremely low transmission latency of URLLC also introduces an inevitable channel estimation error at the receiver, since the pilot length for channel training is very short [30]. Inspired by these features above, there have been several related literatures focused on the theoretical analysis and resource allocation for URLLC systems with short-packet characteristic and imperfect channel state information (CSI). For instance, the pilot-assisted transmission design for URLLC system with zero-forcing (ZF) detection and shadow fading was investigated in [31], and the authors in [32] focused on the statistical queueing analysis for pilot-assisted downlink URLLC systems with periodical arrival process and imperfect CSI. In this scenario, the authors in [32] derived the expression of queueing delay violation probability via using the tool of stochastic network calculus. Meanwhile, the authors in [33] considered the application of cell-free (CF) technique in massive multiple-input multiple-output (MIMO)-enabled URLLC systems with limited pilot length, and derived the lower bounds of downlink ergodic data rate in this system. On the other hand, the authors in [34] and [35] considered the security enhancement issue for pilot-assisted URLLC systems in the presence of passive eavesdropping attacks, and provided some ideas for designing the artificial noise (AN)-assisted pilot and data transmission strategies to improve the secrecy performance of URLLC systems in the presence of randomly located eavesdropping nodes and imperfect CSI at the legitimate link.

B. Motivations, Contributions and Organizations

Nevertheless, the VLC-related and URLLC-related solutions provided in the aforementioned works are not applicable to the reliability analysis and transmission design in our considered

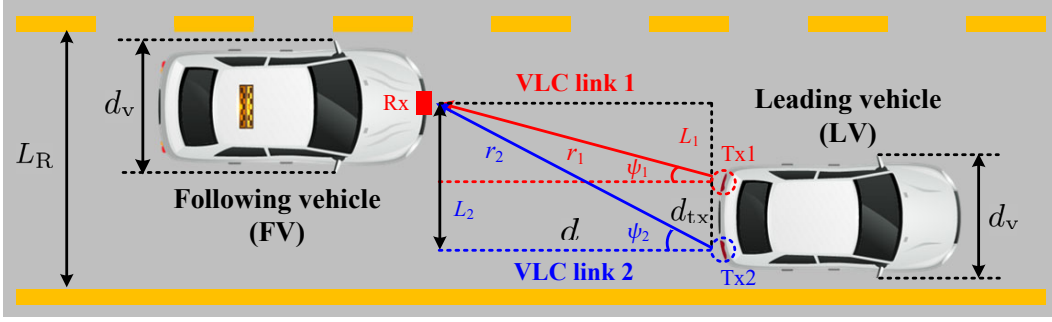


Fig. 1. Graphical representation of outdoor V2V-VLC system model, where the leading vehicle (LV) uses two LED-based taillights Tx1 and Tx2 to transmit the driving safety-related messages in the form of modulated optical data signals, and the following vehicle (FV) utilizes the photodetector Rx installed at the center of bumper to receive the modulated optical data signals.

V2V-VLC system. The main reasons are explained as follows: On the one hand, the VLC-related literatures mentioned above [21]–[28] are based on the ideal assumption of infinite blocklength, which is no longer valid for URLLC system with short codeword blocklength. On the other hand, the URLLC-related literatures mentioned above [31]–[35] are in the category of the RF-based transmission design, which is not applicable for our V2V-VLC system. To the best of our knowledge, the reliability analysis and transmission design for URLLC in outdoor V2V-VLC system, is still an open research issue.

Against the above backgrounds, the main focus of this paper is to provide some preliminary ideas for this unresolved issue. Specifically, we focus on the deployment of VLC technology to enable the driving safety-related URLLC services in outdoor infrastructure-less vehicular systems. Here, we assume that the safety message dissemination is performed in the V2V manner, i.e., the leading vehicle (LV) uses its own LED-based taillights to transmit the driving safety-related messages in the form of modulated optical URLLC signals, and the following vehicle (FV) uses the photodetector to decode the received optical data signal. In fact, the short-packet feature of URLLC introduces an inevitable decoding error and a non-zero channel estimation error, which greatly deteriorates the reliability performance of URLLC. Based on the descriptions above, the contributions of this manuscript are summarized as follows:

- 1) Without loss of generality, we first introduce a composite fading model to describe the propagation environment in the outdoor V2V-VLC scenarios, in which the quality of received optical data signal is degraded by the path loss, atmospheric turbulence, ambient-induced shot noise and thermal noise. Based on this composite fading model, we investigate the reliability performance of our V2V-VLC system in the idea case of perfect CSI, and calculate the average packet loss probability in this circumstance.
- 2) In practical V2V-VLC systems, the channel estimation error is inevitable due to the limited pilot length and the Doppler effect. Inspired by this, we extend the reliability analysis to the V2V-VLC system with imperfect CSI at receiver. Specifically, the analytical expression of packet loss probability in this circumstance is derived via using the numerical integrations and special functions, and the closed-form approximation of packet loss probability is

also presented via using the first-order approximation of Gaussian Q -function and Gauss-Chebyshev quadrature.

Moreover, numerical results illustrate how the average packet loss probability of URLLC in outdoor V2V-VLC system under different atmospheric conditions varies with some parameters, and provide some enlightening conclusions.

The rest of this paper is organized as follows: In Section II, we introduce the outdoor V2V-VLC system model considered in this paper, and provide some basic preliminaries. Then, the reliability performance of V2V-VLC system in the idea case of perfect CSI is analyzed in Section III, and we further analyze the reliability performance of practical V2V-VLC system with imperfect CSI in Section IV. Numerical results and discussions are provided in Section V, and this manuscript is concluded in Section VI.

II. SYSTEM MODEL AND PRELIMINARIES

Here, we are interested in the driving safety-related URLLC applications (e.g., cooperative awareness and emergency warning) in a roadside V2V-VLC system, and the system model is depicted in Fig. 1. In this system, we assume that two vehicles follow each other in a highway segment with a width of L_R . In particular, the leading vehicle (LV) periodically collects some internal information (e.g., speed, position and road condition), and delivers these mission-critical information to the following vehicle (FV) in the form of modulated optical URLLC signals. Meanwhile, the width of each vehicle is equivalent to d_v , and the LV-FV longitudinal distance is set to d . For the transceiver structure, we assume that the LV utilizes its two taillights Tx1 and Tx2 as VLC transmitters, and a photodetector Rx installed at the center of the bumper of FV is employed as VLC receiver. Also, Tx1 and Tx2 are horizontally separated with a distance of d_{tx} , and the propagation distance of VLC links $i = \{1, 2\}$ from Tx i to Rx is expressed as $r_i \triangleq \sqrt{d^2 + L_i^2}$, where L_i is the lateral shift of Tx i relative to Rx. For ease of notation, we denote the LV-FV relative lateral shift as $L = (L_1 + L_2)/2$, and we have $L \leq L_R - d_v$.

Remark 1. Here, we consider the V2V-VLC paradigm in the context of urban road traffic environment. For convenience, the LV and FV in Fig. 1 can be treated as stationary nodes within the transmission duration (e.g., less than 1ms) of each driving safety-related URLLC message. In fact, even when the LV and

FV are driving at the maximal allowable speed of 120km/h in urban road areas, the movement distance of LV and FV within one millisecond is only 3.33cm. Hence, the movement distance of LV and FV during the transmission process of each URLLC message is much less than 3.33cm, which is negligible in the theoretical analysis of our considered V2V-VLC system. ■

A. Error Probability of Short-Packet Communications

In typical URLLC-related V2V systems, the mission-critical information is encoded into short codewords to guarantee the millisecond-level latency requirement. Therefore, it is assumed that each URLLC message sent from the LV must be delivered within a target deadline of $m_s = \tau B$ (channel uses), where τ is the codeword blocklength in the time domain, and B (Hz) is the available bandwidth. Seen from the information-theoretical results in [29], the maximal achievable rate of URLLC system with given codeword blocklength m_s and target decoding error constraint $\varpi_s \in (0, 1)$, is tightly approximated by [29, Eq. (2)]

$$\mathcal{R}_s(\gamma) = \log_2(1 + \gamma) - \sqrt{\frac{\mathcal{V}(\gamma)}{m_s}} \mathcal{Q}^{-1}(\varpi_s), \quad (1)$$

where γ is the effective SNR at the Rx, $\mathcal{V}(\gamma) = (\log_2 e)^2(1 - (1 + \gamma)^{-2})$ is the channel dispersion, and $\mathcal{Q}^{-1}(\cdot)$ is the inverse of Gaussian Q -function with $\mathcal{Q}(z) = \frac{1}{\sqrt{2\pi}} \int_z^\infty e^{-t^2/2} dt$. Then, we introduce the concept of average packet loss probability to characterize the reliability performance of our system, which is defined as the probability that the URLLC message with given payload size of \mathcal{L} cannot be successfully decoded at Rx within the given latency bound m_s . Therefore, the average packet loss probability of our V2V-VLC system is accordingly obtained as

$$\varpi = \int_0^\infty \mathcal{Q}\left(\frac{\log_2(1 + z) - \mathcal{L}/m_s}{\sqrt{\mathcal{V}(z)/m_s}}\right) f_\gamma(z) dz, \quad (2)$$

where $f_\gamma(z)$ represents the probability density function (PDF) of instantaneous effective received SNR γ .

B. VLC Channel Model

In particular, the URLLC data signals $\mathbf{y} = [y_1, y_2]^T \in \mathbb{R}^{2 \times 1}$ received by Rx is mathematically written as

$$\mathbf{y} = \kappa \mathbf{h} x + \mathbf{z}, \quad (3)$$

where $\kappa > 0$ is the responsivity of photodetector, and x stands for the optical signal transmitted by the LV. Here, we assume that $\mathbb{E}[|x|^2] = \rho_T$ in which ρ_T is the transmit electrical power. Meanwhile, $\mathbf{h} = [h_1, h_2]^T$ is the channel state vector of VLC links $i \in \{1, 2\}$, and each element in $\mathbf{h} \in \mathbb{R}^{2 \times 1}$ is modelled as

$$h_i = \beta_i \nu_i, \quad i \in \{1, 2\} \quad (4)$$

where β_i is the path loss coefficient related to the geographical location, and ν_i is the propagation loss component caused by the outdoor atmospheric turbulence. On the one hand, the path loss coefficient of outdoor V2V-VLC systems can be expressed as [36]

$$\beta_i = \frac{(m+1)\mathcal{A}_R}{2\pi r_i^2} \cos^m(\theta_i) \mathcal{T}(\psi_i) g(\psi_i) \cos \psi_i, \quad (5)$$

where $m \triangleq -\ln(2)/\ln(\cos(\Theta_{1/2}))$ is the order of Lambertian emission, and $\Theta_{1/2}$ indicates the semi-angle of Tx1 and Tx2. Meanwhile, \mathcal{A}_R is the detection area of Rx, θ_i and ψ_i indicate the angle-of-irradiance and angle-of-incidence of the VLC link $i \in \{1, 2\}$, respectively. Seen from the layout in Fig. 1, we can derive that $\cos \theta_i = \cos \psi_i = d/r_i$. Apart from this, $\mathcal{T}(\psi_i)$ and $g(\psi_i)$ stand for the optical filter gain and optical concentrator gain, respectively. Specifically, the expression of $g(\psi_i)$ is given as follows:

$$g(\psi_i) = \begin{cases} \frac{n^2}{\sin^2(\Psi_{\text{FOV}})}, & 0 \leq \psi_i \leq \Psi_{\text{FOV}}, \\ 0, & \psi_i > \Psi_{\text{FOV}}, \end{cases} \quad (6)$$

where Ψ_{FOV} denotes the field-of-view (FOV) of photodetector Rx, and $n > 0$ is the refractive index of optical concentrator. On the other hand, the propagation loss component of outdoor V2V-VLC systems is modelled as a random variable following the gamma-gamma distribution. Therefore, the PDF of ν_i can be expressed as [37]

$$f_{\nu_i}(z) = \frac{2(a_i b_i)^{\frac{a_i + b_i}{2}}}{\Gamma(a_i) \Gamma(b_i)} z^{\frac{a_i + b_i}{2} - 1} K_{a_i - b_i}(2\sqrt{a_i b_i z}), \quad (7)$$

where $\Gamma(\cdot)$ stands for the Gamma function [38, Eq. (8.310-1)], and $K_\nu(\cdot)$ is the modified Bessel function of second kind with order ν [38, Eq. (8.407-1)]. Meanwhile, the parameters a_i and b_i that related to the atmospheric conditions are given by

$$a_i = \left(\exp \left[\frac{0.49\omega_i^2}{(1 + 0.18\vartheta_i^2 + 0.56\omega_i^{12/5})^{7/6}} \right] - 1 \right)^{-1}, \quad (8)$$

$$b_i = \left(\exp \left[\frac{0.51\omega_i^2(1 + 0.69\omega_i^{12/5})^{-5/6}}{(1 + 0.9\vartheta_i^2 + 0.62\vartheta_i^2\omega_i^{12/5})^{5/6}} \right] - 1 \right)^{-1}, \quad (9)$$

where $\omega_i^2 \triangleq 0.5\mathcal{C}_0^2 \varrho^{7/6} r_i^{11/6}$, $\vartheta_i^2 \triangleq \varrho \mathcal{D}_0^2 / (4r_i)$ and $\varrho \triangleq 2\pi/\lambda$. Notice that λ denotes the carrier wavelength, \mathcal{D}_0 is the aperture diameter of Rx, and \mathcal{C}_0^2 is the refractive structure parameter.

Remark 2. As mentioned above, the photodetector installed at the center of the bumper of FV has a constrained FOV angle Ψ_{FOV} . Meanwhile, the VLC transmitters of LV have a limited semi-angle $\Theta_{1/2}$. Together with the layouts in Fig. 2, we can obtain that the VLC links become unserviceable as long as the LV-FV relative lateral shift of this system is beyond the safety-critical threshold $L_{\text{th}} \triangleq d \tan(\min(\Theta_{1/2}, \Psi_{\text{FOV}})) + \frac{d_{\text{tx}}}{2}$. That is, if there exists $L > L_{\text{th}}$, it can be deemed that the photodetector is located in the “dead zone” region of VLC and cannot receive the modulated optical signals from the LV. More details will be illustrated through numerical results. ■

C. Additive Noise Model

In particular, $\mathbf{z} = [z_1, z_2]^T$ in (3) denotes the additive noise vector, where each element z_i with $i \in \{1, 2\}$ is modelled as a real-valued Gaussian variable with zero mean and variance σ_i^2 . In practical outdoor V2V-VLC systems, the additive noise z_i is composed of two main components, namely, thermal noise and shot noise. Hence, the variance of z_i is mathematically written as [39]

$$\sigma_i^2 = \sigma_{\text{th}}^2 + \sigma_{i,\text{shot}}^2, \quad (10)$$

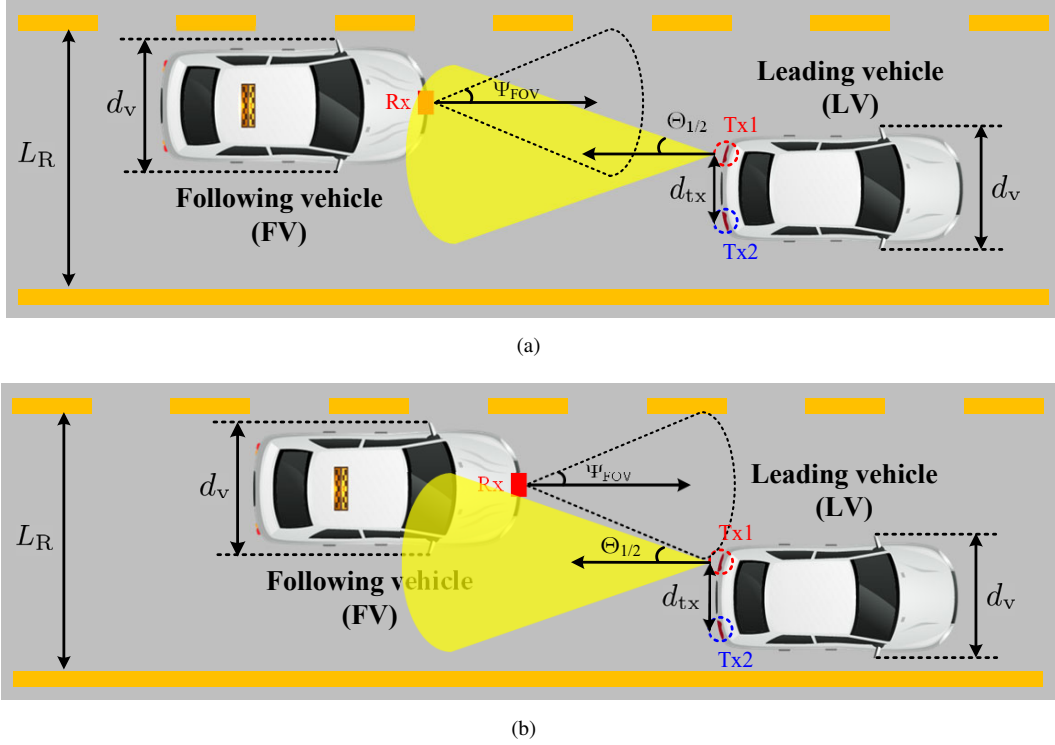


Fig. 2. Diagram of LV-FV misalignment and the safety-critical threshold L_{th} of LV-FV relative lateral shift. Here, we have $L_{th} \triangleq d \tan(\min(\Theta_{1/2}, \Psi_{FOV})) + d_{tx}/2$: (a) The case of $L \leq L_{th}$, i.e., the VLC links are serviceable and the photodetector Rx can receive the modulated optical signals, and (b) The case of $L > L_{th}$, i.e., the photodetector Rx is located in the “dead zone” region such that the VLC links become unserviceable.

where σ_{th}^2 and $\sigma_{i,shot}^2$ are the variances of thermal noise and shot noise, respectively. On the one hand, the thermal noise of our V2V-VLC system contains two main components, namely, feedback-resistor noise and field-effect-transistor (FET) noise. Therefore, the expression of σ_{th}^2 is written as

$$\sigma_{th}^2 = \underbrace{\frac{8\pi K_B T_a}{G_v} \eta A_R I_2 B^2}_{\text{feedback-resistor noise}} + \underbrace{\frac{16\pi^2 K_B T_a \varphi}{\xi} \eta^2 A_R^2 I_3 B^3}_{\text{FET noise}}, \quad (11)$$

where K_B is the Boltzmann constant, T_a indicates the absolute temperature in Kelvin scale, G_v denotes the open-loop voltage gain, η is the fixed capacitance of Rx per unit area, I_2 and I_3 stand for the noise bandwidth factors, ξ is the transconductance of FET, and φ denotes the FET noise factor. On the other hand, the shot noise of our V2V-VLC system is modelled as

$$\sigma_{i,shot}^2 = 2q\kappa B [\rho_T h_i + I_2 \mu_0 \Omega A_R g(\psi_i) \sin^2(\Psi_{FOV})], \quad (12)$$

where q stands for the electron charge, μ_0 is the transmission coefficient of peak filter, and Ω denotes the irradiance that falls within the spectral range of Rx, i.e.,

$$\Omega = \int_{\lambda_{lw}}^{\lambda_{up}} \mathcal{S}_{\text{peak}} \frac{\Phi(\lambda, T_k)}{\max_{\lambda} \Phi(\lambda, T_k)} d\lambda, \quad (13)$$

where λ_{lw} and λ_{up} refer to the lower and upper spectral limits of the optical bandpass filter at Rx, respectively, $\mathcal{S}_{\text{peak}}$ denotes the peak spectral irradiance, and the function $\Phi(\lambda, T_k)$ stands for the spectral irradiance of Blackbody radiation model. Here, we have $\Phi(\lambda, T_k) \triangleq 2\pi\epsilon c^2 \lambda^{-5} / (e^{\epsilon c / (\lambda K_B T_k)} - 1)$, where ϵ is the Planck constant, c denotes the speed of light, and T_k is the

average temperature of solar surface in Kelvin scale.

III. ANALYTICAL FRAMEWORK FOR URLLC IN V2V-VLC SYSTEMS WITH PERFECT CSI

In this section, we consider the ideal case of perfect CSI at the Rx, and investigate the average packet loss probability of URLLC in this circumstance. Under the assumption of perfect CSI, the received electrical SNR of each VLC link $i \in \{1, 2\}$ is accordingly expressed as $\gamma_i = (\kappa \rho_T h_i)^2 / \sigma_i^2 \triangleq \bar{\gamma}_i h_i^2$, where $\bar{\gamma}_i = (\kappa \rho_T)^2 / \sigma_i^2$. Together with (4) and (7), the PDF of γ_i can be derived via replacing the integral variables and taking some manipulations, and we have

$$f_{\gamma_i}(z) = \frac{[a_i b_i / (\beta_i \sqrt{\bar{\gamma}_i})]^{\frac{a_i + b_i}{2}}}{\Gamma(a_i) \Gamma(b_i)} z^{\frac{a_i + b_i}{4} - 1} \times K_{a_i - b_i} \left(2 \sqrt{\frac{a_i b_i}{\beta_i \sqrt{\bar{\gamma}_i}}} z^{\frac{1}{2}} \right). \quad (14)$$

Meanwhile, we assume that the FV uses the selective combining scheme to maximize the received SNR, and thus the post-processing SNR at Rx is expressed as $\gamma \triangleq \max\{\gamma_1, \gamma_2\}$. Since the spacing between Tx1 and Tx2 is sufficiently large, we can assume that γ_1 and γ_2 are mutually independent. Motivated by this, the average packet loss probability ϖ of URLLC in our

V2V-VLC system is expressed as

$$\varpi = \prod_{i=1}^2 \frac{[a_i b_i / (\beta_i \sqrt{\gamma_i})]^{\frac{a_i+b_i}{2}}}{\Gamma(a_i)\Gamma(b_i)} \int_0^\infty \mathcal{Q}\left(\frac{\log_2(1+z) - \mathcal{L}/m_s}{\sqrt{\mathcal{V}(z)/m_s}}\right) \times z^{\frac{a_i+b_i}{4}-1} K_{a_i-b_i}\left(2\sqrt{\frac{a_i b_i}{\beta_i \sqrt{\gamma_i}}} z^{\frac{1}{2}}\right) dz. \quad (15)$$

Nevertheless, the calculation of Eq. (15) is intractable due to its complicated form. Hence, we attempt to simplify the integral-form expression of ϖ via using a first-order approximation of $\mathcal{Q}\left(\frac{\log_2(1+\gamma) - \mathcal{L}/m_s}{\sqrt{\mathcal{V}(\gamma)/m_s}}\right) \approx \Lambda(\gamma)$ with [40]

$$\Lambda(\gamma) \triangleq \begin{cases} 1, & \gamma \leq \gamma_{lw} \\ \frac{1}{2} - \vartheta_s \sqrt{m_s}(\gamma - \zeta), & \gamma_{lw} < \gamma < \gamma_{up} \\ 0, & \gamma \geq \gamma_{up}, \end{cases} \quad (16)$$

where $\vartheta_s \triangleq \frac{1}{2\pi\sqrt{22\mathcal{L}/m_s-1}}$, $\zeta \triangleq 2\mathcal{L}/m_s - 1$, $\gamma_{lw} \triangleq \zeta - \frac{1}{2\vartheta_s\sqrt{m_s}}$ and $\gamma_{up} \triangleq \zeta + \frac{1}{2\vartheta_s\sqrt{m_s}}$. Taking some manipulations, the packet loss probability ϖ in (15) can be approximated as

$$\varpi \approx \prod_{i=1}^2 \mathbb{E}_{\gamma_i}[\Lambda(\gamma_i)] = \vartheta_s \sqrt{m_s} \prod_{i=1}^2 \int_{\gamma_{lw}}^{\gamma_{up}} F_{\gamma_i}(z) dz, \quad (17)$$

where $F_{\gamma_i}(z) \triangleq \int_0^z f_{\gamma_i}(y) dy$ indicates the cumulative distribution (CDF) of received electrical SNR γ_i . For convenience, the expression of $F_{\gamma_i}(z)$ and its derivation process are provided in the following theorem:

Theorem 1. By replacing the integration variables and taking some manipulations, the expression of $F_{\gamma_i}(z)$ is obtained as

$$F_{\gamma_i}(z) = \frac{1}{\Gamma(a_i)\Gamma(b_i)} G_{1,3}^{2,1} \left[\frac{a_i b_i}{\beta_i} \sqrt{\frac{z}{\gamma_i}} \left| \begin{matrix} 1 \\ a_i, b_i, 0 \end{matrix} \right. \right], \quad (18)$$

where $G_{p,q}^{m,n}[\cdot]$ is the Meijer's G -function [38, Eq. (9.301)].

Proof: Seen from Eq. (17), the general expression of $F_{\gamma_i}(z)$ is mathematically written as

$$F_{\gamma_i}(z) = \frac{[a_i b_i / (\beta_i \sqrt{\gamma_i})]^{\frac{a_i+b_i}{2}}}{\Gamma(a_i)\Gamma(b_i)} \times \underbrace{\int_0^z y^{\frac{a_i+b_i}{4}-1} K_{a_i-b_i}\left(2\sqrt{\frac{a_i b_i}{\beta_i \sqrt{\gamma_i}}} y^{\frac{1}{2}}\right) dy}_{\Xi_i(z)}. \quad (19)$$

By setting $u = (y/z)^{\frac{1}{4}}$ and $\chi_i = [a_i b_i / (\beta_i \sqrt{\gamma_i})]^2$, the integral term $\Xi_i(z)$ is rewritten as

$$\Xi_i(z) = \int_0^1 4z^{\frac{a_i+b_i}{4}} u^{a_i+b_i-1} K_{a_i-b_i}(2(\chi_i z)^{\frac{1}{4}} u) du \stackrel{(a)}{=} \int_0^1 2u^{-1} \chi_i^{-\frac{a_i+b_i}{4}} G_{0,2}^{2,0} \left[\sqrt{\chi_i z} u^2 \left| \begin{matrix} - \\ a_i, b_i \end{matrix} \right. \right] du, \quad (20)$$

where (a) is derived from [38, Eq. (9.34-3)], and we can further derive the following expression via substituting (20) into (19)

and taking some manipulations, i.e.,

$$F_{\gamma_i}(z) = \int_0^1 \frac{2u^{-1}}{\Gamma(a_i)\Gamma(b_i)} G_{0,2}^{2,0} \left[\sqrt{\chi_i z} u^2 \left| \begin{matrix} - \\ a_i, b_i \end{matrix} \right. \right] du \stackrel{(b)}{=} \frac{1}{\Gamma(a_i)\Gamma(b_i)} G_{1,3}^{2,1} \left[\sqrt{\chi_i z} \left| \begin{matrix} 1 \\ a_i, b_i, 0 \end{matrix} \right. \right], \quad (21)$$

where (b) is derived from [38, Eq. (7.811-2)]. Furthermore, we can obtain the expression of $F_{\gamma_i}(z)$ shown in (18) via substituting $\chi_i = [a_i b_i / (\beta_i \sqrt{\gamma_i})]^2$ into (21). ■

Inspired by the result in Theorem 1, we can further derive a closed-form approximation of average packet loss probability ϖ by leveraging the Gauss-Chebyshev quadrature method, and the general expression of Gauss-Chebyshev quadrature is given as follows [41]:

$$\int_a^b g(z) dz \approx \frac{b-a}{2} \sum_{j=1}^N \frac{\pi}{N} \sqrt{1-t_j^2} g\left(\frac{b-a}{2} t_j + \frac{b+a}{2}\right), \quad (22)$$

where N is the number of terms with the complexity-accuracy tradeoff and $t_j = \cos\left(\frac{2j-1}{2N}\pi\right)$. Hence, the average packet loss probability ϖ in the ideal case of perfect CSI is approximated as follows:

$$\varpi = \prod_{i=1}^2 \int_{\gamma_{lw}}^{\gamma_{up}} \frac{\vartheta_s \sqrt{m_s}}{\Gamma(a_i)\Gamma(b_i)} G_{1,3}^{2,1} \left[\frac{a_i b_i}{\beta_i} \sqrt{\frac{z}{\gamma_i}} \left| \begin{matrix} 1 \\ a_i, b_i, 0 \end{matrix} \right. \right] dz \stackrel{(c)}{\approx} \vartheta_s \sqrt{m_s} \prod_{i=1}^2 \frac{\gamma_{up} - \gamma_{lw}}{2\Gamma(a_i)\Gamma(b_i)} \sum_{j=1}^N \frac{\pi}{N} \sqrt{1-t_j^2} \times G_{1,3}^{2,1} \left[\frac{a_i b_i}{\beta_i} \sqrt{\frac{\hat{\gamma}_{lw} t_j + \hat{\gamma}_{up}}{\gamma_i}} \left| \begin{matrix} 1 \\ a_i, b_i, 0 \end{matrix} \right. \right], \quad (23)$$

where (c) is derived via using the Gauss-Chebyshev quadrature method. Meanwhile, we have $\hat{\gamma}_{lw} = \frac{\gamma_{up} - \gamma_{lw}}{2}$, $\hat{\gamma}_{up} = \frac{\gamma_{up} + \gamma_{lw}}{2}$ and $t_j = \cos\left(\frac{2j-1}{2N}\pi\right)$.

Remark 3. To obtain a comparable result, we also investigate the conventional outage probability of V2V-VLC system in the premise of infinite blocklength. Under the ideal assumption of perfect CSI, the outage probability of our V2V-VLC system is mathematically written as

$$\varpi_{out} = \prod_{i=1}^2 F_{\gamma_i}(\gamma_{th}) = \prod_{i=1}^2 \frac{1}{\Gamma(a_i)\Gamma(b_i)} G_{1,3}^{2,1} \left[\frac{a_i b_i}{\beta_i} \sqrt{\frac{\gamma_{th}}{\gamma_i}} \left| \begin{matrix} 1 \\ a_i, b_i, 0 \end{matrix} \right. \right], \quad (24)$$

where $\gamma_{th} = 2\mathcal{L}/m_s - 1$, and the relationship between the finite and infinite blocklength cases will be illustrated via numerical results. ■

IV. ANALYTICAL FRAMEWORK FOR URLLC IN V2V-VLC SYSTEMS WITH IMPERFECT CSI

In practical V2V-VLC systems, the channel estimation error is inevitable due to the limited pilot length and Doppler effect. Therefore, the impact of channel estimation error on the V2V-VLC system performance should be taken into consideration to gain a comprehensive insight. In this section, we consider the V2V-VLC system with short-packet feature and imperfect CSI,

and analyze the reliability performance of URLLC in this case. Under the assumption of imperfect CSI, the estimated value of h_i is mathematically written as [42]

$$\tilde{h}_i = \phi h_i + \sqrt{1 - \phi^2} \epsilon_i, \quad (25)$$

where $\phi \in [0, 1]$ denotes a parameter that related to the channel estimation accuracy, and $\phi = 1$ corresponds to the special case of perfect CSI. Meanwhile, the estimation error ϵ_i is modelled as a zero-mean Gaussian random variable with variance of $\sigma_{\epsilon,i}^2$, and we assume that h_i and ϵ_i are mutually independent. Also, the received electrical SNR of each VLC link $i \in \{1, 2\}$ with imperfect CSI is expressed as $\tilde{\gamma}_i = (\kappa \rho_T \tilde{h}_i)^2 / \sigma_i^2 \triangleq \tilde{\gamma}_i h_i^2$, and we recall that $\gamma_i = (\kappa \rho_T)^2 / \sigma_i^2$. Through some manipulations, the PDF of $\tilde{\gamma}_i$ is presented in the following theorem:

Theorem 2. By replacing the integration variables and taking some manipulations, the expression of $f_{\tilde{\gamma}_i}(z)$ is obtained as

$$f_{\tilde{\gamma}_i}(z) = \frac{C_i \left(\sqrt{\frac{z}{\tilde{\gamma}_i}} \right) \sum_{k=0}^{\infty} \frac{(-1)^k}{k!} \mathcal{A}_{i,k} \left(\sqrt{\frac{z}{\tilde{\gamma}_i}} \right) \mathcal{B}_{i,k} \left(\sqrt{\frac{z}{\tilde{\gamma}_i}} \right)}{2\Gamma(a_i)\Gamma(b_i)\sqrt{2\pi(1-\phi^2)\tilde{\gamma}_i z \sigma_{\epsilon,i}}}, \quad (26)$$

where $\mathcal{A}_{i,k}(z)$, $\mathcal{B}_{i,k}(z)$ and $C_i(z)$ are respectively given by

$$\mathcal{A}_{i,k}(z) = \left[\frac{(1-\phi^2)\sigma_{\epsilon,i}^2}{2z^2} \right]^k, \quad (27)$$

$$\mathcal{B}_{i,k}(z) = G_{1,2}^{2,1} \left[-\frac{a_i b_i}{\phi \beta_i} (1-\phi^2)\sigma_{\epsilon,i}^2 z^{-1} \middle| \begin{matrix} 1-2k \\ a_i, b_i \end{matrix} \right], \quad (28)$$

and

$$C_i(z) = \exp \left(-\frac{z^2}{2(1-\phi^2)\sigma_{\epsilon,i}^2} \right). \quad (29)$$

Proof: Seen from Eq. (25), the estimated channel gain \tilde{h}_i is the sum of two random variables. For convenience, we denote $X_i = \phi h_i$ and $Y_i = \sqrt{1 - \phi^2} \epsilon_i$, and we have $\tilde{h}_i = X_i + Y_i$. By replacing the variables and taking some manipulations, the PDFs of X_i and Y_i are respectively expressed as

$$f_{X_i}(z) = \frac{2[a_i b_i / (\phi \beta_i)]^{\frac{a_i+b_i}{2}}}{\Gamma(a_i)\Gamma(b_i)} z^{\frac{a_i+b_i}{2}-1} K_{a_i-b_i} \left(2\sqrt{\frac{a_i b_i}{\phi \beta_i}} z \right), \quad (30)$$

and

$$f_{Y_i}(z) = \frac{1}{\sqrt{2\pi(1-\phi^2)\sigma_{\epsilon,i}}} \exp \left(-\frac{z^2}{2(1-\phi^2)\sigma_{\epsilon,i}^2} \right). \quad (31)$$

Based on the convolution theorem, the PDF of \tilde{h}_i is given by

$$f_{\tilde{h}_i}(z) = \int_0^{\infty} f_{X_i}(y) f_{Y_i}(z-y) dy, \quad (32)$$

and we can further derive the following expression via substituting (30) and (31) into (32):

$$f_{\tilde{h}_i}(z) = \frac{2[a_i b_i / (\phi \beta_i)]^{\frac{a_i+b_i}{2}} \exp \left(-\frac{z^2}{2(1-\phi^2)\sigma_{\epsilon,i}^2} \right)}{\Gamma(a_i)\Gamma(b_i)\sqrt{2\pi(1-\phi^2)\sigma_{\epsilon,i}}} \tilde{\Xi}_i^{(1)}(z), \quad (33)$$

where the integral term $\tilde{\Xi}_i^{(1)}(z)$ is equivalent to

$$\begin{aligned} \tilde{\Xi}_i^{(1)}(z) &= \int_0^{\infty} \exp \left(-\frac{y^2}{2(1-\phi^2)\sigma_{\epsilon,i}^2} \right) \exp \left(\frac{zy}{(1-\phi^2)\sigma_{\epsilon,i}^2} \right) \\ &\quad \times y^{\frac{a_i+b_i}{2}-1} K_{a_i-b_i} \left(2\sqrt{\frac{a_i b_i}{\phi \beta_i}} y \right) dy \\ &\stackrel{(d)}{=} \frac{1}{2} \left(\frac{\phi \beta_i}{a_i b_i} \right)^{\frac{a_i+b_i}{2}} \sum_{k=0}^{\infty} \frac{(-1)^k}{k!} \mathcal{A}_{i,k}(z) \mathcal{B}_{i,k}(z), \end{aligned} \quad (34)$$

where (d) is derived via leveraging the transformations in [38, Eq. (1.211-3)], [38, Eq. (7.813-1)] and [38, Eq. (9.34-3)]. Also, the terms $\mathcal{A}_{i,k}(z)$ and $\mathcal{B}_{i,k}(z)$ are respectively given by

$$\mathcal{A}_{i,k}(z) = \left[\frac{(1-\phi^2)\sigma_{\epsilon,i}^2}{2z^2} \right]^k, \quad (35)$$

and

$$\mathcal{B}_{i,k}(z) = G_{1,2}^{2,1} \left[-\frac{a_i b_i}{\phi \beta_i} (1-\phi^2)\sigma_{\epsilon,i}^2 z^{-1} \middle| \begin{matrix} 1-2k \\ a_i, b_i \end{matrix} \right]. \quad (36)$$

Therefore, the expression of $f_{\tilde{h}_i}(z)$ is derived via substituting (34)-(36) into (33), i.e.,

$$f_{\tilde{h}_i}(z) = \frac{C_i(z) \sum_{k=0}^{\infty} \frac{(-1)^k}{k!} \mathcal{A}_{i,k}(z) \mathcal{B}_{i,k}(z)}{\Gamma(a_i)\Gamma(b_i)\sqrt{2\pi(1-\phi^2)\sigma_{\epsilon,i}}}, \quad (37)$$

where $C_i(z) \triangleq \exp \left(-\frac{z^2}{2(1-\phi^2)\sigma_{\epsilon,i}^2} \right)$. Together with $\tilde{\gamma}_i = \tilde{\gamma}_i h_i^2$ and (37), the mathematical expression of $f_{\tilde{\gamma}_i}(z)$ is obtained as

$$f_{\tilde{\gamma}_i}(z) = \frac{C_i \left(\sqrt{\frac{z}{\tilde{\gamma}_i}} \right) \sum_{k=0}^{\infty} \frac{(-1)^k}{k!} \mathcal{A}_{i,k} \left(\sqrt{\frac{z}{\tilde{\gamma}_i}} \right) \mathcal{B}_{i,k} \left(\sqrt{\frac{z}{\tilde{\gamma}_i}} \right)}{2\Gamma(a_i)\Gamma(b_i)\sqrt{2\pi(1-\phi^2)\tilde{\gamma}_i z \sigma_{\epsilon,i}}}, \quad (38)$$

and the proof is completed. \blacksquare

Inspired by the result in Theorem 2, the exact expression of average packet loss probability with imperfect CSI is obtained as follows:

$$\begin{aligned} \tilde{\omega} &= \prod_{i=1}^2 \frac{1}{2\Gamma(a_i)\Gamma(b_i)} \int_0^{\infty} \mathcal{Q} \left(\frac{\log_2(1+z) - \mathcal{L}/m_s}{\sqrt{\mathcal{V}(z)/m_s}} \right) \\ &\quad \times \frac{C_i \left(\sqrt{\frac{z}{\tilde{\gamma}_i}} \right) \sum_{k=0}^{\infty} \frac{(-1)^k}{k!} \mathcal{A}_{i,k} \left(\sqrt{\frac{z}{\tilde{\gamma}_i}} \right) \mathcal{B}_{i,k} \left(\sqrt{\frac{z}{\tilde{\gamma}_i}} \right)}{\sqrt{2\pi(1-\phi^2)\tilde{\gamma}_i z \sigma_{\epsilon,i}}} dz. \end{aligned} \quad (39)$$

Obviously, the calculation of Eq. (39) is also intractable due to its complicated integral form. Using a similar method in (16), the average packet loss probability $\tilde{\omega}$ can be approximated as

$$\tilde{\omega} \approx \vartheta_s \sqrt{m_s} \prod_{i=1}^2 \int_{\gamma_{iw}}^{\gamma_{iup}} F_{\tilde{\gamma}_i}(z) dz, \quad (40)$$

where $F_{\tilde{\gamma}_i}(z) \triangleq \int_0^z f_{\tilde{\gamma}_i}(y) dy$ indicates the CDF of $\tilde{\gamma}_i$. For the sake of convenience, the closed-form expression of $F_{\tilde{\gamma}_i}(z)$ and its derivation process are provided in the following theorem:

Theorem 3. By replacing the integration variables and taking

some manipulations, the expression of $F_{\tilde{\gamma}_i}(z)$ is obtained as

$$F_{\tilde{\gamma}_i}(z) = \frac{\sum_{k=0}^{\infty} \frac{(-1)^k}{k!} \sum_{l=0}^{\infty} \frac{(-1)^l}{l!} \tilde{\mathcal{A}}_{i,k,l}(z) \tilde{\mathcal{B}}_{i,k,l}(z)}{\sqrt{2\pi}\Gamma(a_i)\Gamma(b_i)}, \quad (41)$$

where $\tilde{\mathcal{A}}_{i,k,l}(z)$ and $\tilde{\mathcal{B}}_{i,k,l}(z)$ are respectively given by

$$\tilde{\mathcal{A}}_{i,k,l}(z) = \frac{1}{2^{k+l}} \left[\frac{z}{(1-\phi^2)\sigma_{\epsilon,i}^2 \tilde{\gamma}_i} \right]^{l-k+\frac{1}{2}}, \quad (42)$$

and

$$\begin{aligned} & \tilde{\mathcal{B}}_{i,k,l}(z) \\ &= G_{3,2}^{1,3} \left[-\frac{\phi\beta_i}{a_i b_i (1-\phi^2)\sigma_{\epsilon,i}^2} \sqrt{\frac{z}{\tilde{\gamma}_i}} \left| \begin{matrix} k-2l, 1-a_i, 1-b_i \\ 2k, k-2l-1 \end{matrix} \right. \right]. \end{aligned} \quad (43)$$

Proof: Seen from Eq. (38), the general expression of $F_{\tilde{\gamma}_i}(z)$ is mathematically written as

$$F_{\tilde{\gamma}_i}(z) = \frac{1}{\sqrt{2\pi}\Gamma(a_i)\Gamma(b_i)} \sum_{k=0}^{\infty} \frac{(-1)^k}{k!} \tilde{\Xi}_{i,k}^{(\text{II})}(z), \quad (44)$$

where the integral term $\tilde{\Xi}_{i,k}^{(\text{II})}(z)$ is expressed as

$$\begin{aligned} & \tilde{\Xi}_{i,k}^{(\text{II})}(z) \\ &= \frac{[(1-\phi^2)\sigma_{\epsilon,i}^2 \tilde{\gamma}_i]^k}{2^{k+1} \sqrt{(1-\phi^2)\tilde{\gamma}_i} \sigma_{\epsilon,i}} \int_0^z \exp\left(-\frac{y}{2(1-\phi^2)\sigma_{\epsilon,i}^2 \tilde{\gamma}_i}\right) \\ & \quad \times y^{-(k+\frac{1}{2})} G_{2,1}^{2,1} \left[-\frac{a_i b_i}{\phi\beta_i} (1-\phi^2)\sigma_{\epsilon,i}^2 \sqrt{\frac{\tilde{\gamma}_i}{y}} \left| \begin{matrix} 1-2k \\ a_i, b_i \end{matrix} \right. \right] dy. \end{aligned} \quad (45)$$

By setting $\tilde{u} = (y/z)^{\frac{1}{2}}$ and leveraging [38, Eq. (1.211-3)], the integral term $\tilde{\Xi}_{i,k}^{(\text{II})}(z)$ can be rewritten as

$$\tilde{\Xi}_{i,k}^{(\text{II})}(z) \triangleq \sum_{l=0}^{\infty} \frac{(-1)^l}{l!} \tilde{\mathcal{A}}_{i,k,l}(z) \tilde{\mathcal{B}}_{i,k,l}(z), \quad (46)$$

where the term $\tilde{\mathcal{A}}_{i,k,l}(z)$ is given by

$$\tilde{\mathcal{A}}_{i,k,l}(z) = \frac{1}{2^{k+l}} \left[\frac{z}{(1-\phi^2)\sigma_{\epsilon,i}^2 \tilde{\gamma}_i} \right]^{l-k+\frac{1}{2}}, \quad (47)$$

and the term $\tilde{\mathcal{B}}_{i,k,l}(z)$ is expressed as

$$\begin{aligned} & \tilde{\mathcal{B}}_{i,k,l}(z) \\ & \stackrel{(e)}{=} \int_0^1 \tilde{u}^{2l-k} G_{2,1}^{1,2} \left[-\frac{\phi\beta_i \sqrt{z/\tilde{\gamma}_i}}{a_i b_i (1-\phi^2)\sigma_{\epsilon,i}^2} \tilde{u} \left| \begin{matrix} 1-a_i, 1-b_i \\ 2k \end{matrix} \right. \right] d\tilde{u} \\ & \stackrel{(f)}{=} G_{3,2}^{1,3} \left[-\frac{\phi\beta_i}{a_i b_i (1-\phi^2)\sigma_{\epsilon,i}^2} \sqrt{\frac{z}{\tilde{\gamma}_i}} \left| \begin{matrix} k-2l, 1-a_i, 1-b_i \\ 2k, k-2l-1 \end{matrix} \right. \right], \end{aligned} \quad (48)$$

where (e) is derived from [38, Eq. (9.31-2)], and (f) is derived from [38, Eq. (7.811-2)]. Therefore, we can further acquire the following expression via substituting (46)-(48) into (44):

$$F_{\tilde{\gamma}_i}(z) = \frac{\sum_{k=0}^{\infty} \frac{(-1)^k}{k!} \sum_{l=0}^{\infty} \frac{(-1)^l}{l!} \tilde{\mathcal{A}}_{i,k,l}(z) \tilde{\mathcal{B}}_{i,k,l}(z)}{\sqrt{2\pi}\Gamma(a_i)\Gamma(b_i)}, \quad (49)$$

TABLE I
SIMULATION PARAMETERS OF V2V-VLC SYSTEM

Parameter	Notation	Value
LED semi-angle	$\Theta_{1/2}$	60°
Detection area of Rx	\mathcal{A}_R	0.8 cm ²
Optical filter gain	$\mathcal{T}(\psi_i)$	1
Refractive index	n	1.5
FOV of Rx	Ψ_{FOV}	60°
Responsivity of photodetector	κ	0.54 A/W
Boltzmann constant	K_B	1.38×10^{-23} J/W
Absolute temperature	T_a	298 K
Open-loop voltage gain	G_v	10
Capacitance per unit area	η	112 pF/cm ²
Noise bandwidth factors	I_2	0.562
	I_3	0.0868
FET transconductance	ξ	30 mS
FET noise factor	φ	1.5
Electron charge	q	1.602×10^{-19} C
Peak filter coefficient	μ_0	1
Lower spectral limit	λ_{lw}	380 nm
Upper spectral limit	λ_{up}	780 nm
Planck constant	ε	6.63×10^{-34} J.s
Speed of light	c	3×10^8 m/s
Average solar surface temperature	T_k	6000 K
Variance of estimation error	$\sigma_{\epsilon,i}^2$	0.1

and the proof is completed. ■

Inspired by the result in Theorem 3, we can further derive a closed-form approximation of average packet loss probability with imperfect CSI as follows:

$$\begin{aligned} \tilde{\omega} &= \prod_{i=1}^2 \int_{\gamma_{\text{lw}}}^{\gamma_{\text{up}}} \frac{\vartheta_s \sqrt{m_s}}{\sqrt{2\pi}\Gamma(a_i)\Gamma(b_i)} \sum_{k=0}^{\infty} \frac{(-1)^k}{k!} \sum_{l=0}^{\infty} \frac{(-1)^l}{l!} \\ & \quad \times \tilde{\mathcal{A}}_{i,k,l}(z) \tilde{\mathcal{B}}_{i,k,l}(z) dz \\ & \stackrel{(g)}{\approx} \prod_{i=1}^2 \frac{\vartheta_s \sqrt{m_s} (\gamma_{\text{up}} - \gamma_{\text{lw}})}{2\sqrt{2\pi}\Gamma(a_i)\Gamma(b_i)} \sum_{k=0}^{\infty} \frac{(-1)^k}{k!} \sum_{l=0}^{\infty} \frac{(-1)^l}{l!} \sum_{j=1}^N \frac{\pi}{N} \\ & \quad \times \sqrt{1-t_j^2} \tilde{\mathcal{A}}_{i,k,l}(\hat{\gamma}_{\text{lw}} t_j + \hat{\gamma}_{\text{up}}) \tilde{\mathcal{B}}_{i,k,l}(\hat{\gamma}_{\text{lw}} t_j + \hat{\gamma}_{\text{up}}), \end{aligned} \quad (50)$$

where (g) is derived via using the similar method in Eq. (23). Meanwhile, we recall that $\hat{\gamma}_{\text{lw}} = \frac{\gamma_{\text{up}} - \gamma_{\text{lw}}}{2}$, $\hat{\gamma}_{\text{up}} = \frac{\gamma_{\text{up}} + \gamma_{\text{lw}}}{2}$ and $t_j = \cos\left(\frac{2j-1}{2N}\pi\right)$.

Remark 4. Similar to Eq. (24), the outage probability of our V2V-VLC system in the premise of imperfect CSI is given by

$$\tilde{\omega}_{\text{out}} = \prod_{i=1}^2 \frac{\sum_{k=0}^{\infty} \frac{(-1)^k}{k!} \sum_{l=0}^{\infty} \frac{(-1)^l}{l!} \tilde{\mathcal{A}}_{i,k,l}(\gamma_{\text{th}}) \tilde{\mathcal{B}}_{i,k,l}(\gamma_{\text{th}})}{\sqrt{2\pi}\Gamma(a_i)\Gamma(b_i)}, \quad (51)$$

and recall that $\gamma_{\text{th}} = 2^{\mathcal{L}/m_s} - 1$. ■

V. NUMERICAL AND SIMULATION RESULTS

In this section, we show the average packet loss probability of URLLC in our considered V2V-VLC system under different atmospheric turbulence conditions, including the weak, moderate and strong turbulences [43]. Moreover, the impact of some

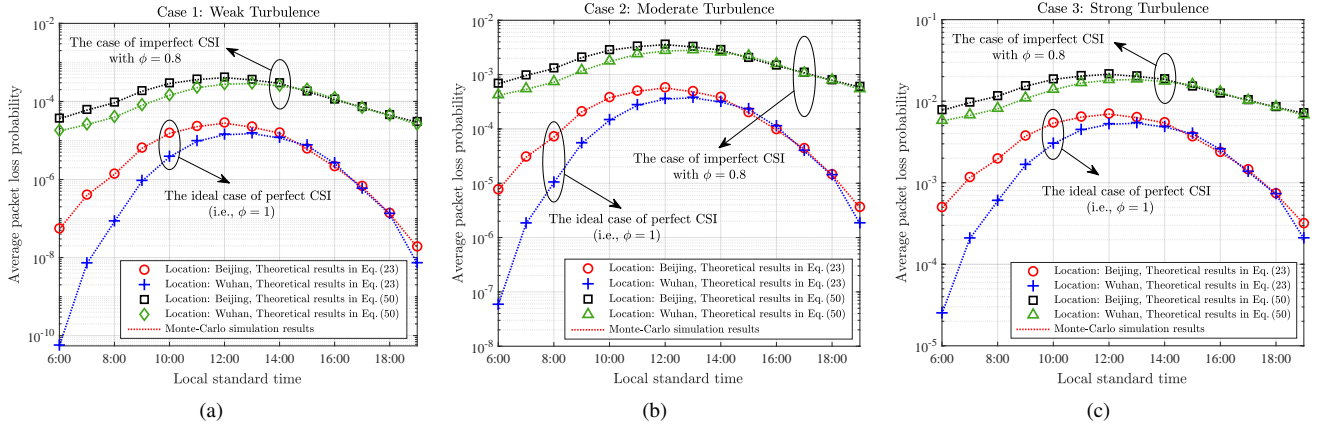


Fig. 3. The average packet loss probability of URLLC in the outdoor V2V-VLC system under different local standard time and atmospheric conditions, where $m_s = 400$ (channel uses) and the LV-FV relative lateral shift is set to $L = 10\text{m}$.

TABLE II
THE MEASURED PEAK SPECTRAL IRRADIANCE IN BEIJING, CHINA [45]

Time	6:00	7:00	8:00	9:00	10:00	11:00	12:00
S_{peak}	86.35	153.43	220.24	347.86	454.12	513.84	547.69
Time	13:00	14:00	15:00	16:00	17:00	18:00	19:00
S_{peak}	508.74	456.31	342.65	250.91	178.19	112.42	63.58

TABLE III
THE MEASURED PEAK SPECTRAL IRRADIANCE IN WUHAN, CHINA [46]

Time	6:00	7:00	8:00	9:00	10:00	11:00	12:00
S_{peak}	10.43	48.01	98.12	195.98	298.48	393.84	442.97
Time	13:00	14:00	15:00	16:00	17:00	18:00	19:00
S_{peak}	453.05	418.47	365.28	266.57	171.41	111.51	48.11

particular transmission parameters (e.g., codeword blocklength and transmit power of optical data signals, LV-FV longitudinal distance and relative lateral shift, channel estimation accuracy, semi-angle of Tx and FOV angle of Rx) is also investigated. Unless otherwise specified, the main simulation parameters are presented as follows: In this system, the LV and FV following each other in a four-lane road segment with the width of $L_R = 15\text{m}$, and the width of each vehicle is set to $d_v = 2\text{m}$ [44]. The transmit power of optical data signals is equal to $\rho_T = 20\text{dBW}$, the LV-FV longitudinal distance is equal to $d = 50\text{m}$, and the horizontal spacing between Tx1 and Tx2 is set to $d_{\text{tx}} = 1.5\text{m}$. On the other hand, we assume that each URLLC message sent from LV contains $\mathcal{L} = 256$ information bits, the total available bandwidth is set to $B = 20\text{MHz}$, and the system parameters related to the VLC channel gain and additive noise are listed in Table I. To emulate the impact of solar irradiance in outdoor V2V-VLC scenarios, the measured peak spectral irradiances in Beijing [45] and Wuhan [46], China are employed to evaluate the system performance, which are given in Tables II and III, respectively. Moreover, all the simulation results are calculated by averaging 10,000 channel realizations.

Seen from an overall perspective, the curves in Fig. 3-Fig. 7

indicate that the theoretical results calculated by Eqs. (23) and (50) roughly coincide with the Monte-Carlo simulation results. Therefore, we can conclude that the theoretical framework in this manuscript is accurate to evaluate the average packet loss probability of URLLC in outdoor V2V-VLC systems. On the other hand, it can be clearly seen that the average packet loss probability of our V2V-VLC system is at a relatively high level in the case of stronger atmospheric turbulence and vice versa. Therefore, we can summarize that the atmospheric turbulence has a significant negative impact on the reliability performance of URLLC in the outdoor V2V-VLC environment. In addition, it can also be observed that the average packet loss probability of V2V-VLC system in the ideal case of perfect CSI is always lower than that of imperfect CSI.

In Fig. 3, we demonstrate the average packet loss probability of URLLC in our V2V-VLC system with different atmospheric conditions and peak spectral irradiance. To gain more insights, we employ the measured values of peak spectral irradiance in two representative regions in China, i.e., Beijing (located in the area of North China) and Wuhan (located in the area of central China). On the one hand, it can be seen from Table II that the peak spectral irradiance of Beijing changes with the local time and achieves the maximal value at the Beijing standard time of 12:00. Apparently, the increase of peak spectral irradiance will lead to the degradation of reliability performance, owing to the background noise from solar radiation. Therefore, the average packet loss probability of outdoor V2V-VLC system in Beijing also achieves the maximal value at 12:00 of the local standard time. On the other hand, it can be observed from Table III that the peak spectral irradiance of Wuhan has a maximal value at the Wuhan standard time of 13:00, and the average packet loss probability of outdoor V2V-VLC system achieves the maximal value at this time. Based on the discussions above, we can find that the geographic location and local time have a significant impact on the reliability performance of V2V-VLC system. In other words, the impact of solar irradiance is indispensable for the reliability analysis of URLLC in our considered V2V-VLC system.

In Fig. 4, we demonstrate the average packet loss probability of URLLC in our V2V-VLC system under different transmit

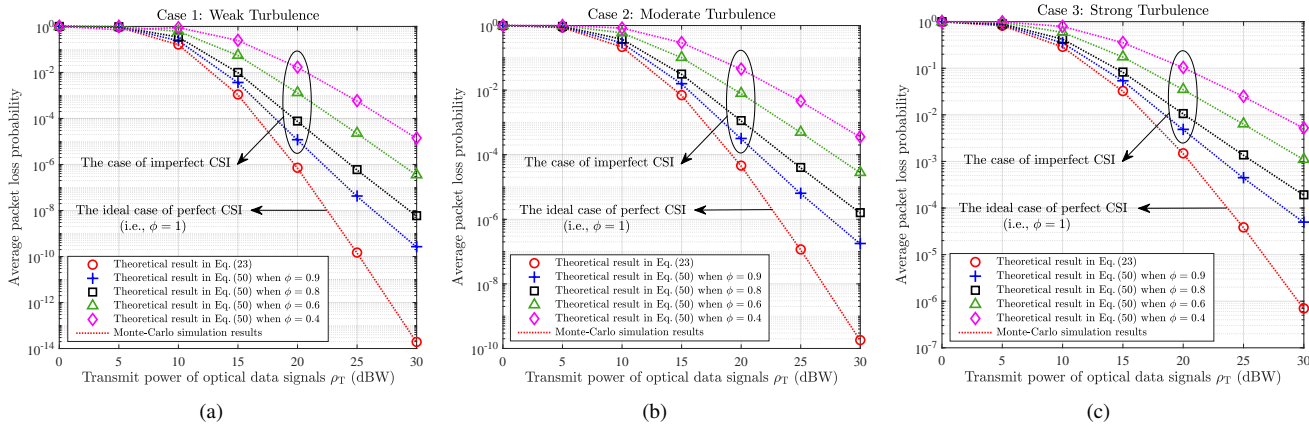


Fig. 4. The average packet loss probability of URLLC in the outdoor V2V-VLC system vs. the transmit power of optical data signals ρ_T (dBW), where $m_s = 400$ (channel uses), the LV-FV relative lateral shift is set to $L = 10\text{m}$. Also, we have $\phi = \{0.4, 0.6, 0.8, 0.9\}$ (i.e., imperfect CSI) and $\phi = 1$ (i.e., perfect CSI). Moreover, the measured peak spectral irradiance in Beijing at 17:00 (i.e., $S_{\text{peak}} = 178.19\text{ W/m}^2$) is employed as the reference value of solar irradiance.

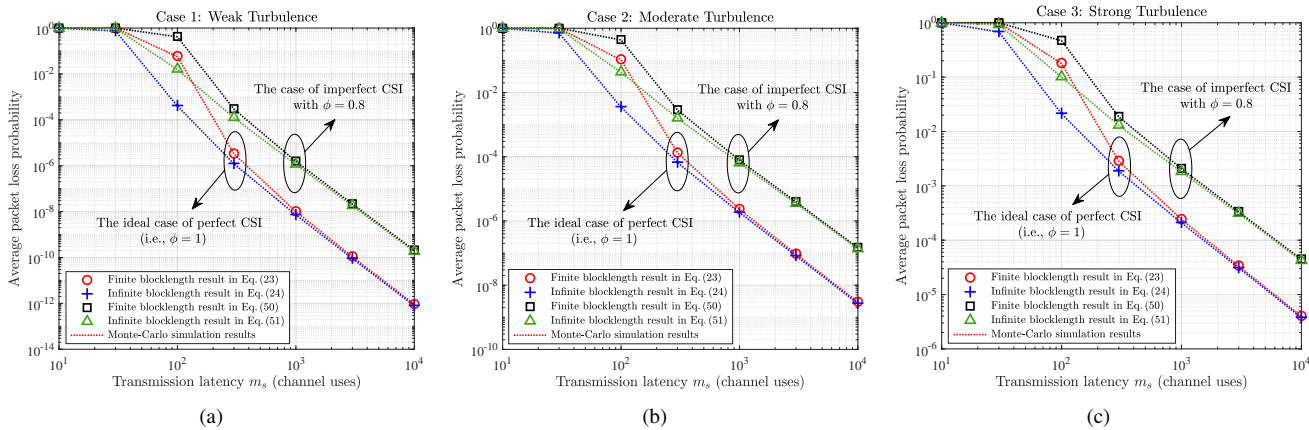


Fig. 5. The average packet loss probability of URLLC in the outdoor V2V-VLC system vs. the transmission latency (i.e., codeword blocklength) m_s (channel uses), where the LV-FV relative lateral shift is set to $L = 10\text{m}$ and the peak spectral irradiance is set to $S_{\text{peak}} = 178.19\text{ W/m}^2$.

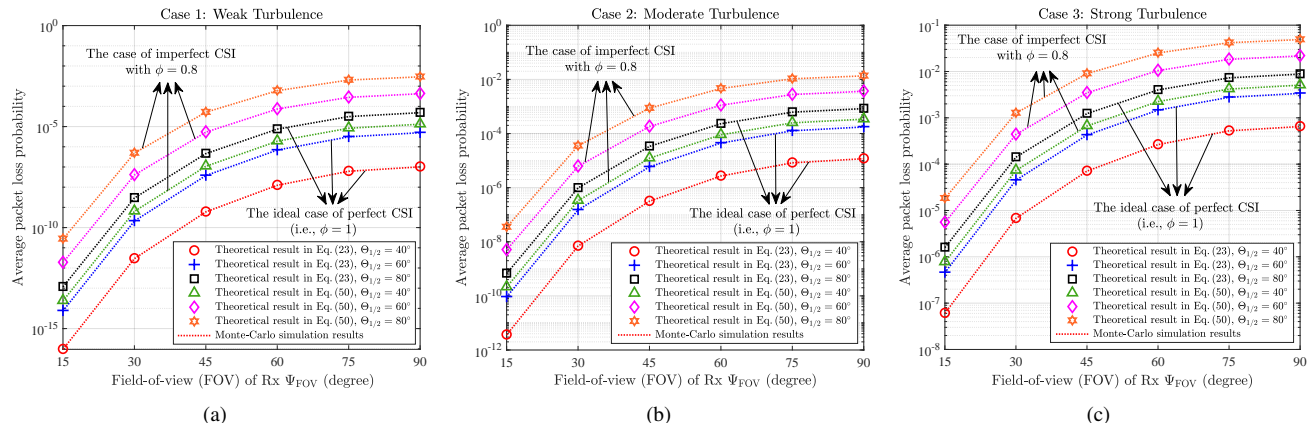


Fig. 6. The average packet loss probability of URLLC in the outdoor V2V-VLC system vs. the field-of-view (FOV) angle Ψ_{FOV} (degree), where $m_s = 400$ (channel uses), the LV-FV relative lateral shift is equal to $L = 10\text{m}$, the peak spectral irradiance is equal to $S_{\text{peak}} = 178.19\text{ W/m}^2$ and the LED semi-angle of VLC transmitters is set to $\Theta_{1/2} = \{40^\circ, 60^\circ, 80^\circ\}$.

power of optical data signals ρ_T (dBW), where the measured peak spectral irradiance in Beijing at the local standard time of 17:00 (i.e., $S_{\text{peak}} = 178.19\text{ W/m}^2$) is adopted as the reference value of solar irradiance in outdoor V2V-VLC environment. It can be clearly observed that the average packet loss probability

of our V2V-VLC system significantly declines as the transmit power ρ_T becomes higher, due to the received electrical SNR at each VLC link is accordingly improved. Meanwhile, we can clearly observe that a higher transmit power should be assigned to the optical data signal for ensuring the reliability constraint

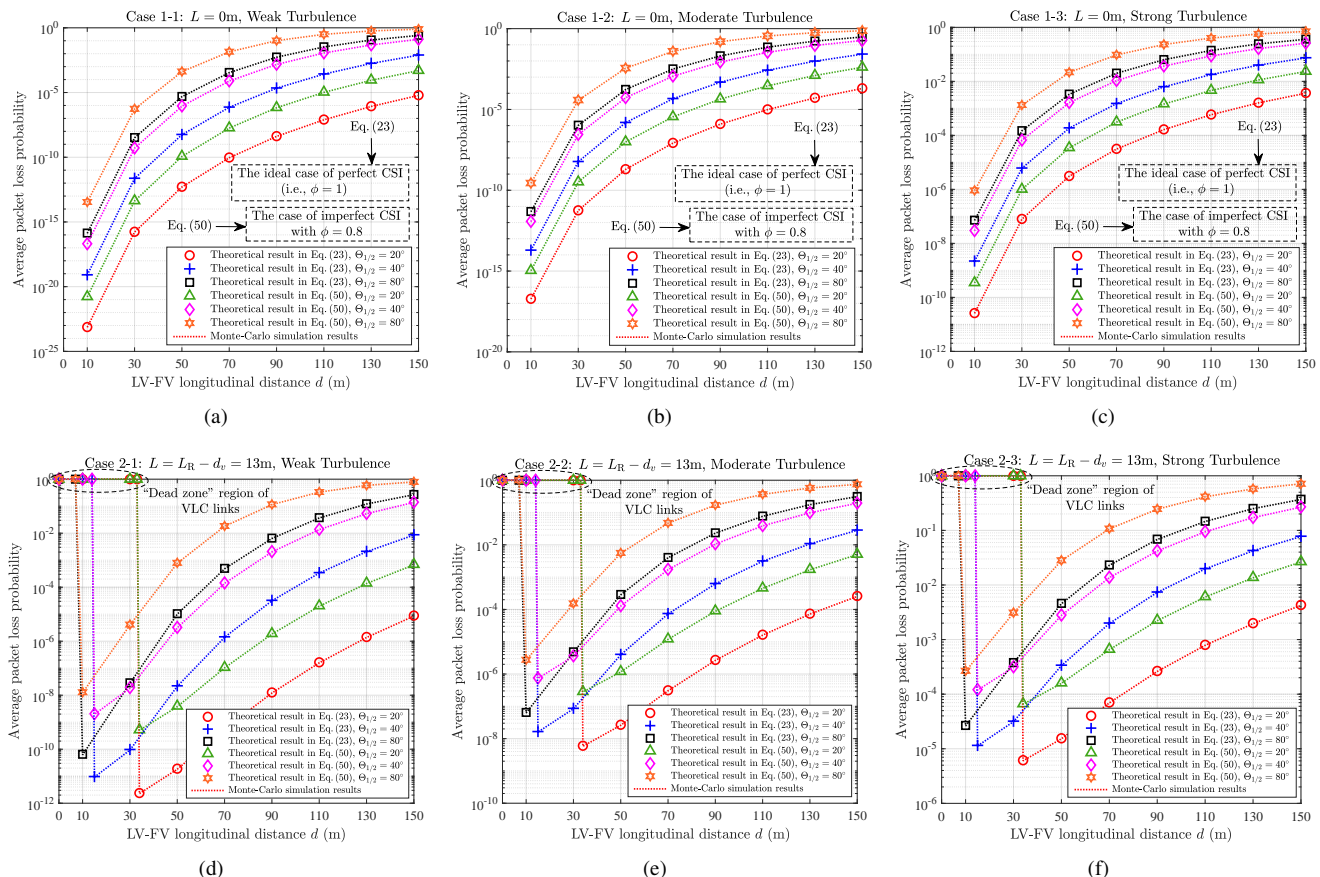


Fig. 7. The average packet loss probability of URLLC in the outdoor V2V-VLC system vs. the LV-FV longitudinal distance d (m), where $m_s = 400$ (channel uses), the peak spectral irradiance is set to $S_{\text{peak}} = 178.19 \text{ W/m}^2$ and the LED semi-angle of VLC transmitters is set to $\Theta_{1/2} = \{20^\circ, 40^\circ, 80^\circ\}$.

when the atmospheric turbulence is stronger. That is, a higher transmit power is required to overcome the negative impact of atmospheric turbulence in the outdoor V2V-VLC environment. In addition, it can also be clearly seen that the average packet loss probability of URLLC in V2V-VLC system rises sharply as the parameter ϕ becomes smaller. That is, the degradation of channel estimation accuracy severely deteriorates the overall reliability of URLLC in the outdoor V2V-VLC system.

In Fig. 5, we demonstrate the impact of transmission latency (i.e., the codeword blocklength) on the reliability performance of URLLC in our V2V-VLC system. Similar to the settings in Fig. 4, the average packet loss probability of URLLC system in Beijing at the local standard time of 17:00 is employed as the reference metric. Firstly, the average packet loss probability of our V2V-VLC system significantly declines as the increase of m_s , due to the required data rate \mathcal{L}/m_s becomes smaller. That is, the reliability performance of our V2V-VLC system can be improved via loosing the latency bound. Secondly, the average packet loss probability that derived from the finite-blocklength information theory is much higher than the traditional outage probability with the ideal assumption of infinite blocklength, and aforementioned gap become smaller as the increase of m_s . Seen from this phenomenon, we can draw the conclusion that the conventional outage probability is no longer applicable to measure the degree of reliability loss of URLLC in our V2V-VLC system, due to it vastly overestimates the achievable rate

of short-packet communications.

In Fig. 6, we demonstrate the average packet loss probability of URLLC in V2V-VLC systems under different field-of-view (FOV) angle Ψ_{FOV} of photodetector Rx and LED semi-angle $\Theta_{1/2}$ of VLC transmitters. On the one hand, it can be observed that the average packet loss probability of outdoor V2V-VLC system significantly decreases when the LED semi-angle $\Theta_{1/2}$ becomes narrower. Apparently, when the VLC transmitters use a narrower light beam, the photodetector Rx is able to capture more transmit power, which implies that the received electrical SNR at each VLC link is accordingly improved. On the other hand, the average packet loss probability of outdoor V2V-VLC system gradually increases when the FOV angle Ψ_{FOV} of Rx becomes wider. In practical, the photodetector Rx with a wider FOV angle can collect more transmit power of optical signals. However, a wider FOV angle also implies that the background noise from solar radiation is amplified. Obviously, in our V2V-VLC system, the negative impact of amplified solar radiation noise is dominant when the FOV angle becomes wider, which severely deteriorates the reliability performance of URLLC.

In Fig. 7, we demonstrate the average packet loss probability of URLLC in our considered V2V-VLC system under different LV-FV longitudinal distance d and relative lateral shift L . On the one hand, it can be clearly observed that the average packet loss probability of our V2V-VLC system rises as the increases of LV-FV longitudinal distance and relative lateral shift, which

implies that the path loss and Tx-Rx misalignment will lead to a severe degradation of reliability performance of URLLC in the outdoor V2V-VLC environment. On the other hand, it can be seen from Figs. 7(d)-7(f) that the packet loss probability of URLLC is always equal to one when the LV-FV longitudinal distance d is lower than a threshold $d_{th} \triangleq \frac{L-d_{tx}/2}{\tan(\min(\Theta_{1/2}, \Psi_{FOV}))}$ for each given LV-FV relative lateral shift L . That is, if $d < d_{th}$ holds, the photodetector Rx is said to be located in the “dead zone” region of VLC links and cannot receive the modulated optical data signals from the LV. Apparently, the range of this region is related to the minimal value between the FOV angle and LED semi-angle, i.e., $\min(\Theta_{1/2}, \Psi_{FOV})$. Meanwhile, the decline of $\min(\Theta_{1/2}, \Psi_{FOV})$ will lead to the augmentation of “dead zone” region of VLC links. Seen from this phenomenon, we can conclude that designing an appropriate combination of LED semi-angle $\Theta_{1/2}$ and FOV angle Ψ_{FOV} is fundamental to ensure the accessibility of V2V-VLC paradigm in the outdoor wireless environment.

VI. CONCLUSION

In this manuscript, we focused on the driving safety-related URLLC services (e.g., cooperative awareness and emergency warning) in an outdoor V2V-VLC system with short codeword blocklength. Firstly, we introduced a composite fading model to describe the propagation environment in the outdoor V2V-VLC scenarios, in which the impacts of path loss, atmospheric turbulence, ambient-induced shot noise and thermal noise were considered. Under this composite fading model, we proposed the concept of average packet loss probability to characterize the reliability performance in this system. Then, we developed a theoretical framework to analyze the packet loss performance of URLLC in the outdoor V2V-VLC system. In particular, we first considered the idea case of perfect CSI, and derived the analytical expression of average packet loss probability. Then, we extended the theoretical framework to the practical V2V-VLC systems with imperfect CSI. Meanwhile, the closed-form expressions of average packet loss probability were provided to simplify the calculation. Numerical results depicted how the average packet loss probability of our V2V-VLC system under different atmospheric conditions changes with specific system parameters, and verified that the theoretical framework in this research work is accurate to calculate the average packet loss probability of URLLC in the outdoor V2V-VLC system. More importantly, this manuscript provided some preliminary ideas for supporting driving safety-related IoV services in the future wireless networks.

ACKNOWLEDGEMENT

The authors would like to thank the anonymous reviewers for their insightful comments and suggestions.

Amir Hussain acknowledges the support of the UK Engineering and Physical Sciences Research Council (EPSRC) - Grants Ref. EP/M026981/1, EP/T021063/1, EP/T024917/1.

REFERENCES

- [1] World Health Organization, “Global status report on road safety 2018,” no. 9789241565684, 2018. [Online]. Available: <https://www.who.int/publications/i/item/9789241565684>

- [2] F. Jameel, Z. Chang, J. Huang and T. Ristaniemi, “Internet of autonomous vehicles: Architecture, features, and socio-technological challenges,” *IEEE Wireless Commun.*, vol. 26, no. 4, pp. 21-29, Aug. 2019.
- [3] W. Miao, G. Min, X. Zhang, Z. Zhao and J. Hu, “Performance modelling and quantitative analysis of vehicular edge computing with bursty task arrivals,” *IEEE Trans. Mobile Comput.*, vol. 22, no. 2, pp. 1129-1142, Feb. 2023.
- [4] H. Yang, K. Zheng, K. Zhang, J. Mei and Y. Qian, “Ultra-reliable and low-latency communications for connected vehicles: Challenges and solutions,” *IEEE Netw.*, vol. 34, no. 3, pp. 92-100, May-Jun. 2020.
- [5] X. Zhang, H. Huang, H. Yin, D. O. Wu, G. Min and Z. Ma, “Resource provisioning in the edge for IoT applications with multilevel services,” *IEEE Internet Things J.*, vol. 6, no. 3, pp. 4262-4271, Jun. 2019.
- [6] J. Park *et al.*, “Extreme ultra-reliable and low-latency communication,” *Nat. Electron.*, vol. 5, no. 3, pp. 133-141, Mar. 2022.
- [7] H. Yang, K. Zheng, L. Zhao and L. Hanzo, “Twin-timescale radio resource management for ultra-reliable and low-latency vehicular networks,” *IEEE Trans. Veh. Technol.*, vol. 69, no. 1, pp. 1023-1036, Jan. 2020.
- [8] M. S. Bahbahani, E. Alsusa and A. Hammadi, “A directional TDMA protocol for high throughput URLLC in mmWave vehicular networks,” *IEEE Trans. Veh. Technol.*, vol. 72, no. 3, pp. 3584-3599, Mar. 2023.
- [9] S. Nayak and S. Roy, “Novel markov chain based URLLC link adaptation method for 5G vehicular networking,” *IEEE Trans. Veh. Technol.*, vol. 70, no. 12, pp. 12302-12311, Dec. 2021.
- [10] S. Samarakoon, M. Bennis, W. Saad and M. Debbah, “Distributed federated learning for ultra-reliable low-latency vehicular communications,” *IEEE Trans. Commun.*, vol. 68, no. 2, pp. 1146-1159, Feb. 2020.
- [11] C. Pan *et al.*, “Asynchronous federated deep reinforcement learning-based URLLC-aware computation offloading in space-assisted vehicular networks,” *IEEE Trans. Intell. Transp. Syst.*, early access, 2022, doi: 10.1109/TITS.2022.3150756.
- [12] T. Yamazato *et al.*, “Vehicle motion and pixel illumination modeling for image sensor based visible light communication,” *IEEE J. Sel. Areas Commun.*, vol. 33, no. 9, pp. 1793-1805, Sep. 2015.
- [13] B. Aly, M. Elamassie and M. Uysal, “Vehicular VLC system with selection combining,” *IEEE Trans. Veh. Technol.*, vol. 71, no. 11, pp. 12350-12355, Nov. 2022.
- [14] G. Li *et al.*, “Position-dependent MIMO demultiplexing strategy for high-speed visible light communication in Internet of vehicles,” *IEEE Internet Things J.*, vol. 9, no. 13, pp. 10833-10850, Jul. 2022.
- [15] I. Takai, T. Harada, M. Andoh, K. Yasutomi, K. Kagawa and S. Kawahito, “Optical vehicle-to-vehicle communication system using LED transmitter and camera receiver,” *IEEE Photon. J.*, vol. 6, no. 5, pp. 1-14, Oct. 2014.
- [16] A. Memedi and F. Dressler, “Vehicular visible light communications: A survey,” *IEEE Commun. Surveys Tuts.*, vol. 23, no. 1, pp. 161-181, 1st Quart., 2021.
- [17] Y. H. Kim, W. A. Cahyadi and Y. H. Chung, “Experimental demonstration of VLC-based vehicle-to-vehicle communications under fog conditions,” *IEEE Photon. J.*, vol. 7, no. 6, pp. 1-9, Dec. 2015.
- [18] M. S. Islim *et al.*, “The impact of solar irradiance on visible light communications,” *J. Lightw. Technol.*, vol. 36, no. 12, pp. 2376-2386, Jun. 2018.
- [19] A. Validi, T. Ludwig, A. Hussein and C. Olaverri-Monreal, “Examining the impact on road safety of different penetration rates of vehicle-to-vehicle communication and adaptive cruise control,” *IEEE Intell. Transp. Syst. Mag.*, vol. 10, no. 4, pp. 24-34, 2018.
- [20] J. Thota, N. F. Abdullah, A. Doufexi and S. Armour, “V2V for vehicular safety applications,” *IEEE Trans. Intell. Transp. Syst.*, vol. 21, no. 6, pp. 2571-2585, Jun. 2020.
- [21] G. Singh, A. Srivastava and V. A. Bohara, “Stochastic geometry-based interference characterization for RF and VLC-based vehicular communication system,” *IEEE Syst. J.*, vol. 15, no. 2, pp. 2035-2045, Jun. 2021.
- [22] P. Sharda, M. R. Bhatnagar and Z. Ghassemlooy, “Modeling of a vehicle-to-vehicle based visible light communication system under shadowing and investigation of the diversity-multiplexing tradeoff,” *IEEE Trans. Veh. Technol.*, vol. 71, no. 9, pp. 9460-9474, Sep. 2022.
- [23] F. M. Alsalamy, O. C. L. Haas, A. Al-Kinani, C. -X. Wang, Z. Ahmad and S. Rajbhandari, “Impact of dynamic traffic on vehicle-to-vehicle visible light communication systems,” *IEEE Syst. J.*, vol. 16, no. 3, pp. 3512-3521, Sep. 2022.
- [24] F. M. Alsalamy *et al.*, “Impact of vehicle headlights radiation pattern on dynamic vehicular VLC channel,” *J. Lightw. Technol.*, vol. 39, no. 10, pp. 3162-3168, May 2021.
- [25] E. Eso, Z. Ghassemlooy, S. Zvanovec, J. Sathian and A. Gholami, “Fundamental analysis of vehicular light communications and the mitigation

of sunlight noise,” *IEEE Trans. Veh. Technol.*, vol. 70, no. 6, pp. 5932-5943, Jun. 2021.

- [26] K. Illanko and X. Fernando, “Adaptive minimization of direct sunlight noise on V2V-VLC receivers,” in *Proc. IEEE 93rd Veh. Technol. Conf. (VTC-Spring)*, Apr. 2021, pp. 1-6.
- [27] R. Mitra, F. Miramirkhani, V. Bhatia and M. Uysal, “Low complexity least minimum symbol error rate based post-distortion for vehicular VLC,” *IEEE Trans. Veh. Technol.*, vol. 69, no. 10, pp. 11800-11810, Oct. 2020.
- [28] S. Refas *et al.*, “Performance analysis of multi-hop V2V VLC system under atmospheric weather conditions,” in *Proc. 9th Int. Conf. Sci. Electron., Technol. Inf. Telecommun. (SETIT)*, May 2022, pp. 414-419.
- [29] W. Yang, G. Durisi, T. Koch and Y. Polyanskiy, “Quasi-static multiple-antenna fading channels at finite blocklength,” *IEEE Trans. Inf. Theory*, vol. 60, no. 7, pp. 4232-4265, Jul. 2014.
- [30] B. Hassibi and B. M. Hochwald, “How much training is needed in multiple-antenna wireless links?,” *IEEE Trans. Inf. Theory*, vol. 49, no. 4, pp. 951-963, Apr. 2003.
- [31] J. Zeng, T. Lv, R. P. Liu, X. Su, Y. J. Guo and N. C. Beaulieu, “Enabling ultrareliable and low-latency communications under shadow fading by massive MU-MIMO,” *IEEE Internet Things J.*, vol. 7, no. 1, pp. 234-246, Jan. 2020.
- [32] S. Schiessl, J. Gross, M. Skoglund and G. Caire, “Delay performance of the multiuser MISO downlink under imperfect CSI and finite-length coding,” *IEEE J. Sel. Areas Commun.*, vol. 37, no. 4, pp. 765-779, Apr. 2019.
- [33] Q. Peng, H. Ren, C. Pan, N. Liu and M. ElKashlan, “Resource allocation for cell-free massive MIMO-enabled URLLC downlink systems,” *IEEE Trans. Veh. Technol.*, early access, 2023, doi: 10.1109/TVT.2023.3243571.
- [34] Y. Xie, P. Ren and D. Xu, “Security-oriented pilot and data transmission for URLLC in mission-critical IoT scenarios,” *IEEE Internet Things J.*, vol. 10, no. 15, pp. 13697-13715, Aug. 2023.
- [35] Y. Xie, T. Zhang and P. Ren, “Secrecy outage analysis of pilot-assisted URLLC systems with randomly distributed eavesdroppers,” *IEEE Commun. Lett.*, vol. 27, no. 4, pp. 1095-1099, Apr. 2023.
- [36] G. Singh, A. Srivastava, V. A. Bohara, Z. Liu, M. Noor-A-Rahim and G. Ghatak, “Heterogeneous visible light and radio communication for improving safety message dissemination at road intersection,” *IEEE Trans. Intell. Transp. Syst.*, vol. 23, no. 10, pp. 17607-17619, Oct. 2022.
- [37] E. Bayaki, R. Schober and R. K. Mallik, “Performance analysis of MIMO free-space optical systems in Gamma-Gamma fading,” *IEEE Trans. Commun.*, vol. 57, no. 11, pp. 3415-3424, Nov. 2009.
- [38] I. S. Gradshteyn, I. M. Ryzhik, A. Jeffrey, D. Zwillinger and S. Technica, *Table of Integrals, Series, and Products*, 7th ed. New York, NY, USA: Academic, 2007.
- [39] I. E. Lee, M. L. Sim, and F. W.-L. Kung, “Performance enhancement of outdoor visible-light communication system using selective combining receiver,” *IET Optoelectron.*, vol. 3, no. 1, pp. 30-39, 2009.
- [40] B. Makki, T. Svensson, and M. Zorzi, “Finite block-length analysis of the incremental redundancy HARQ,” *IEEE Wireless Commun. Lett.*, vol. 3, no. 5, pp. 529-532, Oct. 2014.
- [41] M. Abramowitz and I. A. Stegun, *Handbook of Mathematical Functions with Formulas, Graphs, and Mathematical Tables*, 9th ed. Washington, USA: US Govt. Print, 1972.
- [42] H. A. Suraweera, P. J. Smith and M. Shafi, “Capacity limits and performance analysis of cognitive radio with imperfect channel knowledge,” *IEEE Trans. Veh. Technol.*, vol. 59, no. 4, pp. 1811-1822, May 2010.
- [43] O. M. S. Al-Ebraheemy, A. M. Salhab, A. Chaaban, S. A. Zummo and M. -S. Alouini, “Precise performance analysis of dual-hop mixed RF/unified-FSO DF relaying with heterodyne detection and two IM-DD channel models,” *IEEE Photon. J.*, vol. 11, no. 1, pp. 1-22, Feb. 2019.
- [44] T. K. Mak, K. P. Laberteaux, R. Sengupta and M. Ergen, “Multichannel medium access control for dedicated short-range communications,” *IEEE Trans. Veh. Technol.*, vol. 58, no. 1, pp. 349-366, Jan. 2009.
- [45] B. Hu, Y. Wang and G. Liu, “Measurements and estimations of photosynthetically active radiation in Beijing,” *Atmos. Res.*, vol. 85, no. 3, pp. 361-371, Feb. 2007.
- [46] L. Wang, W. Gong, Y. Ma, B. Hu and M. Zhang, “Photosynthetically active radiation and its relationship with global solar radiation in central China,” *Int. J. Biometeorol.*, vol. 58, no. 6, pp. 1265-1277, Aug. 2014.



Yuncong Xie (Student Member, IEEE) received the B.S. degree in Optical Information Science and Technology from Changsha University of Science and Technology, P. R. China, in 2016. He is currently pursuing the Ph.D. degree with the School of Information and Communications Engineering, Xi’an Jiaotong University, P. R. China. His current research interests include ultra-reliable and low-latency communications (URLLC), Internet-of-Things, information security and optical wireless communications.



Dongyang Xu (Member, IEEE) received the Ph.D. degree in the Department of Information and Communications Engineering at Xi’an Jiaotong University, P. R. China, in 2019. He is currently an Associate Professor in school of Information and Communications Engineering at Xi’an Jiaotong University. His research interests include wireless communications, quantum security and machine learning. He received the Best Paper Rewards from IEEE CHINA COMMUNICATIONS in 2017. Dr. Xu has hosted and participated in more than ten projects.

He has authored 70+ publications including papers in prestigious journal/conferences such as the IEEE Internet of Things Journal, Transactions on Information Forensics and Security, Transactions on Industrial Informatics, Transactions on Vehicular Technology, International Conference on Communications (ICC), Global Communications Conference (GLOBECOM) etc. He has also served as the Technical Program Committee Member for IEEE/CIC International Conference on Communications in China and GLOBECOM. He is a Member of IEEE and IEEE Communications Society.



Tiantian Zhang (Student Member, IEEE) received the B.S. and MA.Sc degree from the Harbin Institute of Technology, Harbin, P. R. China, in 2015 and 2018, respectively. During 2018-2020, he worked as algorithm engineer in ZTE Corporation, mainly engaged in wireless algorithm research. He is currently pursuing the Ph.D. degree with the Xian Jiaotong University, P. R. China. His current research interests include intelligent signal processing, deep learning for wireless communication, radio fingerprinting and security.



Keping Yu (Member, IEEE) received the M.E. and Ph.D. degrees from the Graduate School of Global Information and Telecommunication Studies, Waseda University, Tokyo, Japan, in 2012 and 2016, respectively. He was a Research Associate, Junior Researcher, Researcher with the Global Information and Telecommunication Institute, Waseda University, from 2015 to 2019, 2019 to 2020, 2020 to 2022, respectively. He is currently an Associate Professor, the Vice Director of Institute of Integrated Science and Technology, and the Director of the Network

Intelligence and Security Laboratory, Hosei University, Japan.

Dr. Yu has hosted and participated in more than ten projects, is involved in many standardization activities organized by ITU-T and ICNRG of IRTF, and has contributed to ITU-T Standards Y.3071 and Supplement 35. He received the IEEE Outstanding Leadership Award from IEEE BigDataSE 2021, the Best Paper Award from IEEE Consumer Electronics Magazine Award 2022 (1st Place Winner), IEEE ICFTIC 2021, ITU Kaleidoscope 2020, the Student Presentation Award from JSST 2014. He has authored more than 200 peer-review research papers and books, including over 80 IEEE/ACM Transactions papers. He is an Associate Editor of IEEE Open Journal of Vehicular Technology, Journal of Intelligent Manufacturing, Journal of Circuits, Systems and Computers, and IEICE Transactions on Fundamentals of Electronics, Communications and Computer Sciences. He has been a Guest Editor for more than 20 journals such as IEEE Transactions on Computational Social Systems, IEEE Journal of Biomedical and Health Informatics, and Renewable & Sustainable Energy Reviews. He served as general co-chair and publicity co-chair of the IEEE VTC2020-Spring 1st EBTSRA workshop, general co-chair of IEEE ICC2020 2nd EBTSRA workshop, general co-chair of IEEE TrustCom2021 3rd EBTSRA workshop, session chair of IEEE ICC2020, ITU Kaleidoscope 2016. His research interests include smart grids, information-centric networking, the Internet of Things, artificial intelligence, blockchain, and information security.



Amir Hussain (Senior Member, IEEE) received the B.Eng. (Highest First Class Hons. with Distinction) and Ph.D. degrees from the University of Strathclyde, Glasgow, U.K., in 1992 and 1997, respectively. He is founding Director of the Centre of AI and Robotics at Edinburgh Napier University, UK. His research interests are cross-disciplinary and industry-led, and aimed at developing cognitive data science and trustworthy AI technologies to engineer the smart industrial and healthcare systems of tomorrow. He has (co)authored around 600 research

publications, including over 300 journal papers and 20 Books/monographs. He has supervised over 40 PhD students and led major national and international projects. He is currently managing research grants totalling over £5Million, including as Lead Principal Investigator for the COG-MHEAR Programme (funded under the UK EPSRC Transformative Healthcare Technologies 2050 Call) that aims to develop truly personalised, multi-modal assistive hearing and communication technology. He is founding Chief Editor of Springer's Cognitive Computation journal and editorial board member for Elsevier's Information Fusion and several IEEE Transactions including on: Neural Networks and Learning Systems; Artificial Intelligence; Systems, Man and Cybernetics (Systems); and Emerging Topics in Computational Intelligence. He has served as General Chair of IEEE WCCI 2020 (the world's largest technical event on computational intelligence, comprising the flagship IJCNN, FUZZ-IEEE and IEEE CEC) and the 2023 IEEE Smart World Congress (featuring six co-located IEEE Conferences). He is an Executive Committee member of the UKCRC (the national expert panel of the IET and the BCS for UK computing research) and Chapter Chair of the IEEE UK and Ireland Industry Applications Society.



Mohsen Guizani (Fellow, IEEE) received the B.S. (with Distinction), M.S., and Ph.D. degrees in electrical and computer engineering from Syracuse University, Syracuse, NY, USA, in 1985, 1987, and 1990, respectively.

He is currently a Professor of Machine Learning and the Associate Provost with Mohamed Bin Zayed University of Artificial Intelligence (MBZUAI), Abu Dhabi, UAE. Previously, he worked in different institutions in the USA. He is the author of ten books and more than 800 publications. His research

interests include applied machine learning and artificial intelligence, Internet of Things, intelligent autonomous systems, smart city, and cybersecurity.

Dr. Guizani has won several research awards, including the "2015 IEEE Communications Society Best Survey Paper Award," the Best ComSoc Journal Paper Award in 2021 as well five best paper awards from ICC and Globecom Conferences. He is also the recipient of the 2017 IEEE Communications Society Wireless Technical Committee Recognition Award, the 2018 AdHoc Technical Committee Recognition Award, and the 2019 IEEE Communications and Information Security Technical Recognition Award. He was listed as a Clarivate Analytics Highly Cited Researcher in Computer Science in 2019, 2020, and 2021. He served as the Editor-in-Chief for IEEE NETWORK and is currently serving on the editorial boards of many IEEE transactions and magazines. He was the Chair of the IEEE Communications Society Wireless Technical Committee and the Chair of the TAOS Technical Committee. He served as the IEEE Computer Society Distinguished Speaker and is currently the IEEE ComSoc Distinguished Lecturer.